

1 **A revisit of parametrization of downward longwave radiation in**
2 **summer over the Tibetan Plateau based on high temporal resolution**
3 **measurements**

4 Mengqi Liu^{a,c}, Xiangdong Zheng^d, Jinqiang Zhang^{a,b,c} and Xiangao Xia^{a,b,c}

5 ^a LAGEO, Institute of Atmospheric Physics, Chinese Academy of Sciences, Beijing,
6 100029, China

7 ^b Collaborative Innovation Center on Forecast and Evaluation of Meteorological
8 Disasters, Nanjing University of Information Science & Technology, Nanjing 210044,
9 China

10 ^c College of Earth and Planetary Sciences, University of Chinese Academy of Sciences,
11 Beijing, 100049, China

12 ^d Chinese Academy of Meteorological Sciences, Chinese Meteorological Bureau,
13 Beijing, 100081, China

14

15

Abstract

The Tibetan Plateau (TP) is one of research hot spots in the climate change research due to its unique geographical location and high altitude. Downward longwave radiation (DLR), as a key component in the surface energy budget, is of practical implications for radiation budget and climate change. A couple of attempts have been made to parametrize DLR over the TP based on hourly or daily measurements and crude clear sky discrimination methods. This study uses 1-minute shortwave and longwave radiation measurements at three stations over TP to parameterize DLR during summer months. Three independent methods are used to discriminate clear sky from clouds based on 1-minute radiation and Lidar measurements. This guarantees strict selection of clear sky samples that is fundamental for the parameterization of clear-sky DLR. Eleven clear-sky and four cloudy DLR parameterizations are examined and locally calibrated. Comparing to previous studies, DLR parameterizations here are shown be characterized by smaller root mean square error (RMSE) and higher coefficient of determination (R^2). Clear-sky DLR can be estimated from the best parametrization with RMSE of $3.8 \text{ W}\cdot\text{m}^{-2}$ and $R^2 > 0.98$. Systematic overestimation of clear-sky DLR by the locally calibrated parametrization in one previous study is found to be approximately $25 \text{ W}\cdot\text{m}^{-2}$ (10%), which is very likely due to potential residual cloud contamination on previous clear-sky DLR parametrization. Cloud-base height under overcast conditions is shown to play an important role in cloudy DLR parameterization, which is considered in the locally calibrated parameterization over the TP for the first time. Further studies on DLR parameterization during nighttime and in seasons except summer are required for our better understanding of the role of DLR in climate change.

41 **1 Introduction**

42 The downward longwave radiation (DLR) at the Earth's surface is the largest
43 component of the surface energy budget, being nearly double the downward shortwave
44 radiation (DSR) (Kiehl and Trenberth, 1997). DLR has shown a remarkable increase
45 during the process of global warming (Stephens et al., 2012). This is closely related to
46 the fact that both a warming and moistening of the atmosphere (especially at the lower
47 atmosphere associated with the water vapor feedback) positively contribute to this
48 change. Understanding of complex spatiotemporal variation of DLR and its implication
49 is necessary for improving weather prediction, climate simulation as well as water
50 cycling modeling. Unfortunately, errors in DLR are considered substantially larger than
51 errors in any of the other components of surface energy balance, which is most likely
52 related to the lack of DLR measurements with high quality (Stephens et al., 2012).

53 The 2-sigma uncertainty of DLR measurement by using a well-calibrated and
54 maintained pygeometer is estimated to be 2.5% or $4 \text{ W} \cdot \text{m}^{-2}$ (Stoffel, 2005). However,
55 global-wide surface observations are very limited, especially in some remote regions.
56 On the other hand, it has been known for almost one century that clear-sky DLR is
57 determined by the bulk emissivity and effective temperature of the overlying
58 atmosphere (Ångström, 1918). Since these two quantities are not easily observed for a
59 vertical column of the atmosphere, clear-sky DLR is widely parameterized as a function
60 of surface air temperature and water vapor density, assuming that the clear sky radiates
61 toward the surface like a grey body at screen-level temperature. Dozens of
62 parameterization formulas of DLR have been developed in which clear-sky effective
63 emissivity (ϵ_c) is a function of the screen-level temperature (T) and water vapor pressure
64 (e) (T and e have the same meaning and unit in following equations if not specified), or
65 simply in the localized coefficients with given functions. Two formulas, i.e., an
66 exponential function (Idso, 1981) and a power law function (Brunt, 1932; Swinbank,
67 1963), have been widely used to depict the relationship of ϵ_c to T and e . The coefficients
68 of these functions are derived by a regression analysis of collocated measurements of
69 T , e and DLR. Most of these proposed parameterizations are empirical in nature and
70 only specific for definite atmospheric condition. An exception is that Brutsaert (1975)

71 developed a model based on the analytic solution of the Schwarzschild's equation for a
72 standard atmospheric lapse rates of T and e . Prata (1996) found that the precipitable
73 water content (w) was much better to represent the effective emissivity of the
74 atmosphere than e , which was loosely based on radiative transfer simulations. Dilley
75 and O'Brien (1998) adopted this scheme but tuned empirically their parameterization
76 using an accurate radiative transfer model. Since DLR is to some extent impacted by
77 water vapor and temperature profile (especially in case of existence of an inversion
78 layer) and diurnal variation of T , a new model with two more coefficients considering
79 these effects was developed (Dupont et al., 2008a).

80 In the presence of clouds, total effective emissivity of the sky is remarkably
81 modulated by clouds. The existing clear-sky parameterization should be modified
82 according to the cloud fraction (CF) and other cloud parameters such as cloud base
83 height (CBH). CF is generally used to represent a fairly simple cloud modification
84 under cloudy conditions. Dozens of equations with cloudiness correction have been
85 developed and evaluated by DLR measurements across the world (Crawford and
86 Duchon, 1999; Niemela et al., 2001). CF can be obtained by trained human observers
87 (Iziomon et al., 2003) or derived from DSR (Crawford and Duchon, 1999) and DLR
88 measurements (Durr and Philipona, 2004). High temporal resolution of DSR or DLR
89 measurements (for example, 1-minute) can also provide cloud type information
90 (Duchon and O'Malley, 1999), and thereby allow to consider potential effects of cloud
91 types on DLR (Orsini et al., 2002).

92 With an average altitude exceeding 4 km above the sea level (ASL), the Tibetan
93 Plateau (TP) exerts a huge influence on regional and global climate through mechanical
94 and thermal forcing because of its highest and most extensive highland in the world
95 (Duan and Wu, 2006). TP, compared to other high altitude regions and the poles, has
96 been relatively more sensitive to climate change. The most rapid warming rate over the
97 TP occurred in the latter half of the 20th century likely associated with relatively large
98 increase in DLR. Duan and Wu (2006) indicated that increase in low level nocturnal
99 cloud amount and thereby DLR could partly explain the increase in the minimum
100 temperature, despite decrease in total cloud amount during the same period. By using

101 observed sensitivity of DLR to change in specific humidity for the Alps, Rangwala et
102 al. (2009) suggested that increase in water vapor appeared to be partly responsible for
103 the large warming over the TP. Since the coefficients of certain empirical
104 parameterizations and their performances showed spatiotemporal variations,
105 establishment of localized DLR parameterizations over the TP is of high significance.
106 Further studies on DLR, including its spatiotemporal variability, its parameterization as
107 well as its sensitivity to changes in atmospheric variables, would be expected to
108 improve our understanding of climate change over the TP (Wang and Dickinson, 2013).

109 DLR measurements from high quality radiometer with high temporal resolution
110 over the TP are quite scarce. To the best of our knowledge, there are very few
111 publications on DLR and its parameterization over the TP. Wang and Liang (2009)
112 evaluated clear-sky DLR parameterizations of Brunt (1932) and Brutsaert (1975) at 36
113 globally distributed sites, in which DLR data at two TP stations were used. Yang et al.
114 (2012) used hourly DLR data at 6 stations to study major characteristics of DLR and to
115 assess the all-sky parameterization of Crawford and Duchon (1999). Zhu et al. (2017)
116 evaluated 13 clear-sky and 10 all-sky DLR models based on hourly DLR measurements
117 at 5 automatic meteorological stations. The Kipp & Zonen CNR1 is composed of CM3
118 pyranometer and CG3 pyrgeometer that are used to measure DLR and DSR,
119 respectively. The CG3 is the second class radiometer according to the International
120 Organization for Standardization (ISO) classification. The root mean square error of
121 hourly DLR is less than $5 \text{ W} \cdot \text{m}^{-2}$ after field recalibration and window heating correction
122 (Michel et al., 2008). Note that human observations of cloud every 3-6 hours or hourly
123 DLR and DSR data are respectively used to determine clear sky and cloud cover in
124 these previous studies.

125 In order to further our understanding of DLR and DSR over the TP, measurements
126 of 1-minute DSR and DLR at 3 stations over the TP using state-of-the-art instruments
127 have been performed in summer months since 2011. These data provide us opportunity
128 to evaluate clear-sky DLR models and quantitatively assess cloud impacts on DLR.
129 This study makes progress in the following aspects as compared to previous studies: 1)
130 clear-sky discrimination and CF estimation are based on 1-minute DSR and DLR

131 measurements that are objective in nature; 2) misclassification of cloudiness into cloud-
132 free skies would be minimized by adopting strict cloud-screening procedures based on
133 1-minute DSR, DLR and Lidar measurements; 3) potential effects of CBH on DLR are
134 also investigated. Localized parameterizations of clear-sky and all-sky DLRs are finally
135 achieved, which would be expected to improve DLR estimations over the TP.

136

137 **2. Site, Instrument and Data**

138 Measurements of DLR and DSR conducted 1~4 months over the TP at three
139 stations (Table 1), including Nagqu (NQ, 92.04°E, 31.29°N, 4507 m ASL), Nyingchi
140 (NC, 94.2°E, 29.4°N, 2290 m ASL) and Ali (AL, 80°E, 32.5°N, 4287 m ASL) are used
141 for the DLR parameterization. DLR and DSR were respectively measured by CG4 and
142 CM21 radiometers (Kipp & Zonen, Delft, Netherlands). The sampling frequency is 1
143 Hz and the averages of the samples over 1-minute intervals are logged on a Campbell
144 Scientific CR23X datalogger. Simultaneous 1-minute averages of T and e are taken
145 from the automatic meteorological stations. With the aid of its specific material and
146 unique construction, CG4 is designed for the DLR measurement with high reliability
147 and accuracy. Window heating due to absorption of solar radiation in the window
148 material, the major error source of DLR measurement, is strongly suppressed by its
149 unique construction conducting away the absorbed heat very effectively. CM21 is a
150 high performance research grade pyranometer. Introduction of individually optimized
151 temperature compensation for CM21 makes it have much a smaller thermal offset than
152 CM3. The installation of the CG4 and CM21 on the Kipp & Zonen CV2 ventilation
153 unit prevents dew deposition on the window of the CG4 and the quartz dome of the
154 CM21. The radiometers are calibrated before and after field measurements to the
155 standards held by the China National Centre for Meteorological Metrology.

156 A Micropulse Lidar (MPL-4B, Sigma Space Corporation, United States) was
157 installed side-by-side with radiometers. The Nd:YLF laser of the MPL produces an
158 output power of 12 μ J at 532 nm. The repetition rate is 2500 Hz. The vertical resolution
159 of the MPL data is 30 m and the integration time of the measurements is 30s. The MPL
160 backscattering profiles are used to identify the cloud boundaries and derive the CBHs

161 (He et al., 2013). The dataset used in this article contains about 700 hours of coincident
162 DLR, DSR, Lidar and meteorological measurements.

163 DLR and DSR were also measured at Lhasa (91.1°E, 29.9°N, 3649 m ASL) during
164 summer in 2012 using the same instruments as those in other stations. Lhasa data are
165 mainly used for independent validation because of no Lidar data there.

166

167 **3. Methods**

168 **3.1 Clear-sky discrimination**

169 Clear skies should be discriminated from cloudy conditions before performing
170 DLR parametrization, which is achieved by the synthetical analysis of DSR, DLR, and
171 CBH from MPL.

172 Following the method initiated by Crawford and Duchon (1999), we calculate two
173 quantities reflecting DSR magnitude and variability based on 1-minute observed DSR
174 (DSR_{obs}) and calculated clear-sky DSR (DSR_{cal}) values. DSR_{cal} is calculated by the
175 model C of Iqbal (1983), in which direct and diffuse DSR are parametrized separately.
176 Direct DSR (DSR_{dir}) is calculated as follows.

$$177 \quad DSR_{dir} = S_0 \tau_r \tau_w \tau_o \tau_a \tau_g \quad (1)$$

178 where τ_r , τ_w , τ_o , τ_a and τ_g are transmittances due to Rayleigh scattering, water
179 vapor absorption, ozone absorption, aerosol extinction and absorption by uniformly
180 mixed gases O₂ and CO₂, respectively. Diffuse radiation is estimated as the sum of
181 Rayleigh and aerosol scattering as well as multiple reflectance. Total ozone column
182 (DU) is provided by Brewer spectrophotometer. w values (cm) are from Vaisala-92
183 radiosonde profiles in AL and Global Position System measurements in NC and NQ,
184 respectively. They are used to create linear regression relationship to collocated ground
185 level e (hPa) measurements, which is then used to estimate w from 1-minute
186 measurements of e . Ångström wavelength exponent and Ångström turbidity are from
187 CE-318 sunphotometer observations in NC and AL, while in NQ we adopt the same
188 value as that in AL because their altitudes are similar. Climatic value of single scattering
189 albedo retrieved from long-period CE-318 observation in Lhasa is 0.90 (Che et al.,
190 2019), which is used in three stations. This is reasonable because of high altitude and

191 extremely low aerosol loading in TP. Surface Albedo is 0.25 and 0.22 in AI and NQ
192 according to in situ measurements (Liang et al., 2012). In NC, it is 0.183 (Zhao et al.,
193 2011).

194 DSR_{cal} values are first scaled to a constant value of $1400 \text{ W}\cdot\text{m}^{-2}$ for each minute of
195 each day. We adopt this value according to Duchon and O'Malley (1998) and Long and
196 Ackerman (2000), which only favors for a clear presentation of the normalized and
197 observed DSR values in the same figure. Afterwards, DSR_{obs} values are scaled by
198 multiplying the same set of scale factors. Finally, the mean and standard deviation of
199 the scaled DSR in a 21-minute moving window (± 10 minute centered on the time of
200 interest) are used for cloud screening. Selection of the width of 21-minute is empirical
201 but a consequence of having a reasonable time span for estimating the mean and
202 variance (Duchon and O'Malley, 1999). Clear-sky DSR should satisfy three
203 requirements: 1) ratio of DSR_{obs} to DSR_{cal} is within 0.95 to 1.05; 2) difference between
204 scaled DSR_{obs} and DSR_{cal} is less than $20 \text{ W}\cdot\text{m}^{-2}$; and 3) standard deviation (δ) of scaled
205 DSR_{obs} in a 21-minute moving window is less than $20 \text{ W}\cdot\text{m}^{-2}$.

206 Temporal variability of DLR is also used for cloud screening according to Marty
207 and Philipona (2000) and Sutter et al. (2004). Here, δ of scaled DLR (scaled to 500
208 $\text{W}\cdot\text{m}^{-2}$) in a 21-minute moving window is used for this purpose. Cloud-free sample is
209 determined if δ is less than $5 \text{ W}\cdot\text{m}^{-2}$.

210 Since both DSR and DLR experience difficulties in detecting clouds in the portion
211 of the sky far away from the sun (Duchon and O'Malley, 1999) or high-altitude cirrus
212 clouds (Dupont et al., 2008b), coincident MPL backscatter measurements are used to
213 strictly select clear-sky samples. There should be a cloud element somewhere in the sky
214 when MPL identifies cloud, it is thus required that no clouds are detected by MPL in a
215 21-minute moving window, otherwise it is defined as cloudy.

216 Given the fact that these methods are complementary to each other to some extent
217 (Orsini et al., 2002), we use the following strategy to guarantee a proper selection of
218 clear-sky samples. If DSR, DLR and MPL measurements at the time of interest
219 synchronously satisfy these specified clear-sky conditions, the sample is thought to be
220 taken under unambiguously cloud-free condition; on the contrary, the measurement are

221 made under unambiguously cloudy condition if any method suggests cloudy. Our
222 following clear-sky and cloudy DLR parameterizations are respectively based on
223 measurements under unambiguously cloud-free (8195 minutes) and cloudy conditions
224 (69318 minutes).

225 Fig. 1 shows an example of clear sky discrimination results based on our method.
226 DSR_{obs} presents a smooth temporal variation from sunrise to about 14:00 (LST), being
227 consistent with DSR_{clr} . Similarly, DLR also varies very smoothly during the same
228 period when 21-minute standard deviations of DLR are $< 5 \text{ W}\cdot\text{m}^{-2}$. Both facts suggest
229 sunny and cloudless skies. This inference is supported by MPL that suggests no cloud
230 detected overhead. Contrarily, abrupt changes of 1-minute DSR_{obs} and DLR are
231 evident during 14:00~17:00 LST and we can see DSR_{obs} occasionally exceeds the
232 expected DSR_{clr} , indicating frequent occurrence of fair weather cumuli clouds. MPL
233 detect a persistent thin cloud layer at 4 km above ground, which agrees with DSR and
234 DLR measurements very well.

235

236 **3.2 Cloud fraction estimation**

237 Given synoptic cloud observations are very limited and temporally sparse, various
238 parameterizations using DSR or DLR data have been developed to estimate CF (e.g.,
239 Deardorff, 1978; Marty and Philipona, 2000; Durr and Philipona, 2004; Long et al.,
240 2006; Long and Turner, 2008). Because of good agreement between clear-sky DSR_{obs}
241 and DSR_{cal} calculated by the Iqbal C calculations (Iqbal, 1983; Gubler et al., 2012),
242 with mean bias of $1.7 \text{ W}\cdot\text{m}^{-2}$ and root mean square error (RMSE) of $10.7 \text{ W}\cdot\text{m}^{-2}$ (not
243 shown), we use Deardorff (1978)'s method to calculate CF from DSR_{obs} and DSR_{cal} .
244 The method is based on a fairly simple cloud modification to DSR as follows.

$$245 \quad CF = 1 - \frac{DSR_{obs}}{DSR_{cal}} \quad (2)$$

246 CF (no unit) has values ranging from 0 to 1. To avoid the error caused by abrupt
247 DSR variation, 21-minute mean DSR value rather than its instantaneous measurements
248 are used here.

249

250 **4 Results**

251 4.1 Clear-sky DLR parameterization evaluation and localization

252 Eleven clear-sky DLR (DLR_{clr}) parameterizations (Table 2) are evaluated based
253 on 1-minute DLR measurements under unambiguously cloud-free conditions. To
254 compare the performance of these 11 models, RMSE and the coefficient of
255 determination (R^2) are shown by a Taylor diagram in Fig. 2(a). Relatively smaller
256 RMSE (generally $< 15 \text{ W} \cdot \text{m}^{-2}$) and larger R^2 (> 0.95) are derived for the Brutsaert (1975);
257 Konzelmann (1994), Dilley and O'Brien (1998) and Prata (1996) models. This is likely
258 because these parameterizations were developed in cool and dry areas, for example, in
259 England (Brutsaert, 1975); in Greenland (Konzelmann, 1994) and dry desert region in
260 Australia (Prata, 1996). The climate in those areas is likely similar to that over the TP
261 to some extent, so those parameterizations are expected to perform well. The higher
262 RMSE ($> 37 \text{ W} \cdot \text{m}^{-2}$) and the lower R^2 (~ 0.7) are derived for Swinbank (1963) and Idso
263 and Jackson (1969) models. This can be partly explained by the fact that only T is used
264 in these two methods. Previous studies suggest substantial uncertainty (RMSE > 37.5
265 $\text{W} \cdot \text{m}^{-2}$ and $R^2 < 0.75$) if water vapor effect on DLR_{clr} is not accounted for (Duarte et al.,
266 2006). Since w is very low over the TP and thereby DLR is highly sensitive to variation
267 of w in that case, much more attention should be paid to water vapor effect on the
268 parameterization of DLR_{clr} .

269 The coefficients in eleven parameterizations (Table 2) were originally calibrated
270 and determined in different geographical locations; therefore, they may not be the
271 optimal values for the TP. Thus we take use of 1-minute clear-sky DLR samples to
272 locally calibrate the parameters of these parametrizations. We use 10-fold cross-
273 validation method to determine the parameters. This is a widely used method to
274 estimate the skill of a regression model on unseen data. It is expected to result in a less
275 biased or less optimistic estimate of the model skill than other methods, such as a simple
276 train/test split (James et al., 2013). All the data was randomly dividing into 10 groups
277 of approximately equal size, the coefficients are computed by using 9 groups as training
278 set, and the remaining 1 group is used as validation. This procedure is repeated 10 times
279 to get the representational value of coefficients (with the lowest test error).

280 The coefficient values derived from the non-linear least-squares fitting of the
 281 DLR_{clr} parameterizations (Table 2) over the TP are presented in Table 3. For each fitted
 282 parameterization, we calculated RMSE and R^2 and the results are shown in Fig. 2b.
 283 When using the parameterizations with the locally fitted parameters, the accuracy of
 284 the parameterization relative to the published values is obviously improved. Most
 285 RMSEs are $< 10 \text{ W} \cdot \text{m}^{-2}$ except the parameterization proposed by Swinbank (1963) and
 286 Idso and Jackson (1969) that still produce the worst results (with R^2 of 0.71 and RMSE
 287 of $15 \text{ W} \cdot \text{m}^{-2}$) even after the parameters are locally calibrated. This is probably because
 288 e is not considered in these two methods.

289 The Dilley and O'Brien (1998)'s parameterization, which is initially developed by
 290 considering the adaptation of climatological diversities, is expected to be able to fit the
 291 measurements in tropical, mid-latitude and Polar Regions. This expectation is verified
 292 by its wide deployment in DLR_{clr} estimations in different climate regimes and altitude
 293 levels, for example, in the tropical lowland (eastern Pará state, Brazil) and the mild
 294 mountain area (Boulder, the United States) (Marthews et al., 2012; Li et al., 2017).
 295 The present study confirms that Dilley and O'Brien (1998) is the best clear-sky
 296 parameterization over the TP. The locally calibrated equation is as follows.

$$297 \quad DLR_{clr} = -2.53 + 158.10 \times \left(\frac{T}{273.16}\right)^6 + 106.40 \times \left(\frac{46.50 \times \frac{e}{T}}{2.50}\right)^{\frac{1}{2}} \quad (3)$$

298 The RMSE and R^2 of Eq.(3) are $\sim 3.8 \text{ W} \cdot \text{m}^{-2}$ and > 0.98 respectively, which are
 299 substantially lower than those in previous studies over the TP, for example, the RMSE
 300 was $9.5 \text{ W} \cdot \text{m}^{-2}$ (Zhu et al., 2017). The Dilley and O'Brien (1998)'s parameterization
 301 was suggested to be the most reliable estimates of DLR_{clr} over the TP (Zhu et al., 2017).
 302 Note that the parameters here differ quite a lot from their values (Zhu et al., 2017), as
 303 shown in Eq. (4).

$$304 \quad DLR_{clr} = 30.00 + 157.00 \times \left(\frac{T}{273.16}\right)^6 + 97.93 \times \left(\frac{46.50 \times \frac{e}{T}}{2.50}\right)^{\frac{1}{2}} \quad (4)$$

305 Fig.3 compares instantaneous clear-sky DLR data from measurements against
 306 calculations by Eq. (3) of this study and by Eq. (4) from Zhu et al. (2017). The former
 307 performs very well as shown by an overwhelmingly large number of data points falling
 308 along or overlapping the 1:1 line. By contrast, the latter overestimates DLR by $25 \text{ W} \cdot \text{m}^{-2}$

309 ² (10%). This difference is not very likely due to different DLR measurements used to
310 produce Eq. (3) and (4) giving the following considerations. First, this systematic
311 overestimation is much larger than the expected uncertainty of DLR measurements (2.5%
312 or $4 \text{ W}\cdot\text{m}^{-2}$) (Stoffel, 2005). More important, comparison of cloudy DLR
313 parameterizations between this study and Zhu et al. (2017) showed good agreement
314 (not shown). Note that only 1-hour CG3 DLR observations are used for clear sky
315 discrimination in Zhu et al. (2017). This method was shown to be very likely
316 contaminated by the thin high cloud (Sutter et al., 2004). This certainly would produce
317 an overestimation of clear sky DLR parameterization since larger DLRs are associated
318 with potential residual clouds relative to real clear-sky DLRs.

319

320 **4.2 Parameterization of cloudy-sky DLR**

321 Parameterizations of cloudy-sky DLR (DLR_{cld}) are based on estimated DLR_{clr}
322 coupled with the effect of cloudiness or cloud emissivity, which depends primarily on
323 CF as well as other cloud parameters, like CBH and cloud type (Arking, 1990; Viúdez-
324 Mora et al., 2015). Four parameterizations (Table 4), which modifies the bulk
325 emissivity depending on CF, are assessed and locally calibrated in this section.

326 DLR_{clr} is estimated according to Eq. (3). The fitted values of the coefficients (using
327 10-Fold Cross-Validation) of the four cloudy parameterizations are presented in Table
328 4. RMSE and R^2 of original and locally fitted parameterizations over the TP are
329 presented in Fig. 4.

330 Relative to clear-sky conditions, cloudy parameterizations using the given
331 parameters have higher error RMSE (generally exceeding $35 \text{ W}\cdot\text{m}^{-2}$) except that
332 developed by Jacobs (1978) (RMSE of $18 \text{ W}\cdot\text{m}^{-2}$). R^2 was generally smaller than 0.9.
333 RMSE values decrease significantly in Maykut and Church (1973) and Sugita and
334 Brutsaert (1993) as locally calibrated parameters are used. Relative smaller and almost
335 no RMSE improvements are found for the methods developed by Konzelmann (1994)
336 and Jacobs (1978).

337 Eq. (5) shows the best cloudy-sky parameterization over the TP by combining the
338 clear-sky parameterization of Dilley and O'Brien (1998) with the cloud modulation

339 correction scheme of Jacobs (1978).

$$340 \quad \text{DLR}_{\text{cloud}} = (1 + 0.23 \times \text{CF}) \times \left(59.38 + 113.70 \times \left(\frac{T}{273.16} \right)^6 + 96.96 \times \left(\frac{46.50 \times \frac{e}{T}}{2.50} \right)^{\frac{1}{2}} \right) \quad (5)$$

341 RMSE and R^2 are $\sim 18 \text{ W} \cdot \text{m}^{-2}$ and ~ 0.89 respectively. RMSE here is close to $15 \text{ W} \cdot \text{m}^{-2}$
342 obtained in different altitude areas in Swiss (Gubler et al., 2012) and slightly lower than
343 $23 \text{ W} \cdot \text{m}^{-2}$ obtained in mountain area in Germany (Iziomon et al., 2003). Comparing to
344 previous studies over the TP (RMSE of $22 \text{ W} \cdot \text{m}^{-2}$ in Zhu et al., 2017), our cloudy model
345 produces better results.

346 In order to validate the newly developed DLR parameterizations, clear-sky and
347 cloudy-sky DLR parameterizations are validated against DLR measurements at Lhasa.
348 The results are shown in Fig. 5. Compared to the existed parameterizations, the Eq.(3)
349 and Eq.(5) produce the smallest bias (both less than $2 \text{ W} \cdot \text{m}^{-2}$) and RMSE (Eq.(3)'s is
350 less than $5 \text{ W} \cdot \text{m}^{-2}$ and Eq.(5)'s is less than $25 \text{ W} \cdot \text{m}^{-2}$). This independently demonstrates
351 the improved DLR parameterizations can be used in other stations over the TP.

352

353 **4.3 Effect of CBH on DLR under Overcast Conditions**

354 Since clouds behave approximately as a blackbody, the most relevant cloud
355 parameter (besides CF) to DLR under overcast skies (DLR_{ovc}) is CBH (Kato et al, 2011;
356 Viúdez-Mora et al., 2015): firstly, CBH defines the temperature of the lowest cloud
357 boundary, which through the Stefan-Boltzmann law drives the cloud emittance;
358 secondly, DLR emitted by the atmospheric layers above a cloud is totally absorbed by
359 the cloud itself (clouds are thick enough). Radiative transfer model simulation has
360 suggested that CBH under overcast conditions is an important modulator for DLR. The
361 cloud radiation effect (CRE), the difference between DLR_{obs} and DLR_{clr} , decreases with
362 increasing CBH at a rate of $4 \sim 12 \text{ W} \cdot \text{m}^{-2}$ that depends on climate profiles (Viúdez-Mora
363 et al., 2015). This indicates that overcast DLR parameterization would be improved if
364 CBH is considered.

365 A close relationship between CRE and CBH under overcast conditions over the TP
366 is presented in Fig 6. Compared to Viúdez-Mora (2015) results derived at Girona, Spain,
367 a mid-latitude site with low altitude, CRE over the TP is generally lower by $5 \sim 10 \text{ W} \cdot \text{m}^{-2}$

368 ². This is likely because clouds over the TP with the same CBH as that at Girona have
 369 relatively lower temperature, thereby producing lower radiative effect on DLR. CRE
 370 generally decreases as CBH increases. The result agrees with the expectation since
 371 CBH influence on DLR should decrease as CBH increases as a result of increasing
 372 water vapor effects on DLR. According to Fig 6, CRE is about $70 \text{ W}\cdot\text{m}^{-2}$ for clouds <
 373 1 km and decreases to $\sim 40 \text{ W}\cdot\text{m}^{-2}$ for clouds at 3~4 km in TP. The decreasing rate of
 374 CRE with CBH is estimated to be $-9.8 \text{ W}\cdot\text{m}^{-2}\cdot\text{km}^{-1}$ over the TP that agrees with model
 375 simulations (Viúdez-Mora et al., 2015).

376 Since CBH effect on overcast DLR is apparent, we introduced a modified
 377 parameterization to consider CBH effect on DLR under overcast conditions. A linear
 378 correlation is firstly established based on the measured CBH and the ratio of observed
 379 DLR ($\text{DLR}_{\text{ovc}}^{\text{obs}}$) and calculated DLR by Eq.(5) ($\text{DLR}_{\text{ovc}}^{\text{cal}}$) under overcast condition in Fig
 380 6. Since we can see that $\text{DLR}_{\text{ovc}}^{\text{cal}}$ is equal to DLR_{clr} times 1.23 (because CF is equal to
 381 1 in Eq. 5), we derived a CBH corrected DLR_{ovc} parametrization as follows.

$$382 \quad \text{DLR}_{\text{ovc}} = 1.23 \times \text{DLR}_{\text{clr}} \times (1.07 - 0.046 \times \text{CBH}) \quad (6)$$

383 Where CBH has unit of km. The bias and RMSE of Eq. (6) between measurements
 384 and calculations is $-2.15 \text{ W}\cdot\text{m}^{-2}$ and $19.79 \text{ W}\cdot\text{m}^{-2}$, respectively, which are significantly
 385 lower than that of Eq. (5) ($10.3 \text{ W}\cdot\text{m}^{-2}$ and $21.4 \text{ W}\cdot\text{m}^{-2}$) in overcast conditions. The
 386 result indicates a remarkable improvement in the estimation of DLR under overcast
 387 conditions by introducing CBH to the DLR parameterization; therefore, introduction of
 388 such instruments as ceilometer to measure CBH is highly significant for studying
 389 cloud's impacts on DLR.

390

391 **5 Discussion and conclusions**

392 The parameterization of clear-sky DLR requires a well-defined distinction
 393 between clear-sky and cloudy-sky situations that commonly depends on human cloud
 394 observations 4~6 times each day. Human observation is subjective in nature and its low
 395 temporal resolution cannot resolve dramatic high-resolution variation of clouds.
 396 Furthermore, synoptic human cloud observations show the tendency to stronger weight

397 to the horizon that DLR is not highly sensitive (Marty and Philipona, 2004). Clear sky
398 discrimination based on hourly DSR or DLR measurements also tends to be very
399 suspect of residual clouds due to their low temporal resolution. Parameterization of
400 clear-sky DLR based on these two methods is hence very likely biased as a consequence
401 of selection of cloud contaminated clear-sky measurements. This would result in biased
402 estimation of cloud DLR effect since it is the difference between clear-sky and
403 measured all-sky DLRs (Dupont et al., 2008b).

404 Using 1-minute DSR and DLR at 3 stations over the TP, DLR parameterizations
405 are evaluated and localized parameterizations have been developed based on a
406 comprehensive cloud-screening method. We test the fitted parameterizations based on
407 independent DLR measurements at Lhasa. Potential CBH effect on overcast DLR is
408 experimentally determined. Major conclusions are as follows.

409 Among 11 clear-sky DLR parameterizations tested in this study, two methods
410 using only atmospheric temperature largely deviate from other parameterizations. The
411 best method suitable for TP is the parameterization developed by Dilley and O'Brien
412 (1998). DLR estimation can be improved by localization of these parameterizations.
413 Locally calibrated parameterization can produce clear sky DLR with RMSE of 3.8
414 $W \cdot m^{-2}$.

415 Overcast DLR is highly sensitive to CBH. The parameterization can be
416 substantially improved by consideration of CBH effect. The bias between empirically
417 parameterized calculations and measurements decreases from 10.3 to 1.3 $W \cdot m^{-2}$.

418 The focus of this study is on daytime DLR parameterization over the TP since DSR
419 is used in the cloud-screening method. Given a significant role of DLR played in the
420 surface energy budget during nighttime, it is highly desirable to perform further study
421 on the nighttime DLR parametrization. These results are based on summer DLR
422 measurements, so the conclusions here need to be further tested in other seasons,
423 especially in winter when an increasing tendency of DLR has been observed (Rangwala
424 et al., 2009). Further investigations on these issues are expected to shed new light on
425 how and why DLR has changed over the TP. Our results clearly showed substantial
426 CBH effect on overcast DLR, which would be considered in future when ceilometer is

427 widely used to measure CBH.

428

429 Acknowledgements: This work was supported by the Strategic Priority Research
430 Program of Chinese Academy of Sciences (XDA17010101), the National Key R&D
431 Program of China (2017YFA0603504), the National Natural Science Foundation of
432 China (91537213, 91637107, and 41875183), the Special Fund for Meteorological
433 Research in the Public Interest (GYHY201106023), and the Science and Technological
434 Innovation Team Project of Chinese Academy of Meteorological Science (2013Z005)
435 respectively support the observations at AL, NQ and NC. We greatly appreciate Dr. Q.
436 He for providing the MPL Lidar measurement images and derived CBH data.

437 **References**

- 438 Ångström, A.: A study of the radiation of the atmosphere, Smithsonian Miscellaneous
439 Collection, 65, 1–159, 1915.
- 440 Arking, A.: The radiative effects of clouds and their impact on climate, Bull. Am.
441 Meteorol. Soc., 72, 795-813, 10.1175/1520-
442 0477(1991)072<0795:Treoca>2.0.Co;2, 1991.
- 443 Brunt, D.: Notes on radiation in the atmosphere, Q. J. Roy. Meteorol. Soc., 58, 389–
444 420, 1932.
- 445 Brutsaert, W.: On a derivable formula for long-wave radiation from clear skies, Water
446 Resource Res., 11, 742–744, 1975.
- 447 Carmona, F., Rivas, R., and Caselles, V.: Estimation of daytime downward longwave
448 radiation under clear and cloudy skies conditions over a sub-humid region, Theor.
449 Appl. Climatol., 115, 281-295, 10.1007/s00704-013-0891-3, 2014.
- 450 Che, H. Z., Zhao, H. J., Wu, Y. F., Xia, X. G., Zhu, J., Wang, H., Wang, Y. Q., Sun, J.
451 Y., Yu, J., Zhang, X. Y., and Shi, G. Y.: Analyses of aerosol optical properties and
452 direct radiative forcing over urban and industrial regions in Northeast China,
453 Meteorol. Atmos. Phys., 127, 345-354, 10.1007/s00703-015-0367-3, 2015.
- 454 Che, H., Xia, X., Zhao, H., Dubovik, O., Holben, B. N., Goloub, P., Cuevas-Agulló, E.,
455 Estelles, V., Wang, Y., Zhu, J., Qi, B., Gong, W., Yang, H., Zhang, R., Yang, L.,
456 Chen, J., Wang, H., Zheng, Y., Gui, K., Zhang, X., and Zhang, X.: Spatial
457 distribution of aerosol microphysical and optical properties and direct radiative
458 effect from the China Aerosol Remote Sensing Network, Atmos. Chem. Phys.
459 Discuss., <https://doi.org/10.5194/acp-2019-405>, 2019.
- 460 Crawford, T. M., and Duchon, C. E.: An improved parameterization for estimating
461 effective atmospheric emissivity for use in calculating daytime downwelling
462 longwave radiation, J. Appl. Meteorol., 38, 474–480, 1998.
- 463 Deardorff, J. W.: Efficient prediction of ground surface temperature and moisture, with
464 an inclusion of a layer of vegetation. J. Geophys. Res., 83, 1889–1903, 1978.
- 465 Dilley, A. C., and O'Brien, D. M.: Estimating downward clear sky long-wave irradiance
466 at the surface from screen temperature and precipitable water, Q. J. Roy. Meteorol.
467 Soc., 124a, 1391–1401, 1997.
- 468 Dozier, J., and Frew, J.: Rapid calculation of terrain parameters for radiation modeling
469 from digital elevation data, IEEE T. Geosci. Remote, 28, 963–969, 1990.

470 Dominik, M., R. Philipona, C. Ruckstuhl, R. Vogt and L. Vuilleumier, Performance and
471 uncertainty of CNR1 net radiometers during a one-year field comparison, *J of*
472 *Atmos., and Ocean. Tech.*, 25(3), 442-451, 2008.

473 Duan, A., and Wu, G.: Change of cloud amount and the climate warming on the Tibetan
474 Plateau, *Geophys. Res. Lett.*, 33, 10.1029/2006gl027946, 2006.

475 Duarte, H. F., Dias, N. L., and Maggioletto, S. R.: Assessing daytime downward
476 longwave radiation estimates for clear and cloudy skies in Southern Brazil, *Agr.*
477 *Forest. Meteorol.*, 139, 171-181, 10.1016/j.agrformet.2006.06.008, 2006.

478 Duchon, C. E., and O'Malley, M. S.: Estimating cloud type from pyranometer
479 observations, *J. Appl. Meteorol.*, 38, 132-141, 1999.

480 Dupont, J. C., Haeffelin, M., Drobinski, P., and Besnard, T.: Parametric model to
481 estimate clear-sky longwave irradiance at the surface on the basis of vertical
482 distribution of humidity and temperature, *J. Geophys. Res.*, 113,
483 10.1029/2007jd009046, 2008.

484 Durr, B., and Philipona, R.: Automatic cloud amount detection by surface longwave
485 downward radiation measurements, *J. Geophys. Res.*, 109, 9,
486 10.1029/2003jd004182, 2004.

487 Gubler, S., Gruber, S., and Purves, R. S.: Uncertainties of parameterized surface
488 downward clear-sky shortwave and all-sky longwave radiation, *Atmos. Chem.*
489 *Phys.*, 12, 5077-5098, 10.5194/acp-12-5077-2012, 2012.

490 He, Q. S., Li, C. C., Ma, J. Z., Wang, H. Q., Shi, G. M., Liang, Z. R., Luan, Q., Geng,
491 F. H., and Zhou, X. W.: The properties and formation of cirrus clouds over the
492 Tibetan Plateau based on summertime lidar measurements, *J. Atmos. Sci.*, 70, 901-
493 915, 10.1175/jas-d-12-0171.1, 2013.

494 Idso, S. B.: A set of equations for full spectrum and 8 to 14 μm and 10.5 to 12.5 μm
495 thermal radiation from cloudless skies, *Water Resource Res.*, 17, 295–304, 1981.

496 Iqbal, M.: *An Introduction to Solar Radiation*, Academic Press, Toronto, Canada, 1983.

497 Iziomon, M. G., Mayer, H., and Matzarakis, A.: Downward atmospheric longwave
498 irradiance under clear and cloudy skies: measurement and parameterization, *J.*
499 *Atmos. Solar-Terr. Phys.*, 65, 1107–1116, 2003.

500 Jacobs, J.D.: Radiation climate of Broughton Island, in: *Energy Budget Studies in*
501 *Relation to Fast-ice Breakup Processes in Davis Strait*, edited by Barry, R. G. and
502 Jacobs, J. D., *Inst. of Arctic and Alp. Res. Occas. Paper No. 26*. University of
503 Colorado, Boulder, pp. 105–120, 1978.

504 James, G., Witten, D., Hastie, T., and Tibshirani, R.: An Introduction to Statistical
505 Learning: with Applications in R, Springer-Verlag New York, USA, 2013.

506 Kato, S., Rose, F., Sun, S., Miller, W., Chen, Y., Rutan, D., Stephens, G., Loeb, N.,
507 Minnis, P., Wielicki, B., Winker, D., Charlock, T., Stackhouse Jr, P., Xu, K. M.,
508 and Collins, W.: Improvements of top-of-atmosphere and surface irradiance
509 computations with CALIPSO-, CloudSat-, and MODIS-derived cloud and aerosol
510 properties, *J. Geophys. Res.*, 116, D19209, 10.1029/2011JD016050, 2011.

511 Kiehl, J. T., and Trenberth, K. E.: Earth's annual global mean energy budget. *Bull. Am.*
512 *Meteorol. Soc.*, 78, 197-208, 1997.

513 Konzelmann, T., van de Wal, R. S. W., Greuell, W., Bintanja, R., Henneken, E. A. C.,
514 and Abe-Ouchi, A.: Parameterization of global and longwave incoming radiation
515 for the Greenland Ice Sheet, *Global Planet. Change*, 9, 143–164, 1994.

516 Kruk, N. S., Vendrame, I. F., da Rocha, H. R., Chou, S. C., and Cabral, O.: Downward
517 longwave radiation estimates for clear and all-sky conditions in the Sertozinho
518 region of So Paulo, Brazil, *Theor. Appl. Climatol.*, 99, 115-123, 2010.

519 Li, M. Y., Jiang, Y. J., and Coimbra, C. F. M.: On the determination of atmospheric
520 longwave irradiance under all-sky conditions, *Sol. Energy.*, 144, 40-48,
521 10.1016/j.solener.2017.01.006, 2017.

522 Liang, H., Zhang, R. H., Liu, J. M., Sun, Z. A., and Cheng, X. H.: Estimation of hourly
523 solar radiation at the surface under cloudless conditions on the Tibetan Plateau
524 using a simple radiation model, *Adv. Atmos. Sci.*, 29, 675-689, 10.1007/s00376-
525 012-1157-1, 2012.

526 Long, C. N., Ackerman, T. P., Gaustad, K. L., and Cole, J. N. S.: Estimation of fractional
527 sky cover from broadband shortwave radiometer measurements, *J. Geophys. Res.*,
528 111, 11, 10.1029/2005jd006475, 2006.

529 Long, C. N., and Turner, D. D.: A method for continuous estimation of clear-sky
530 downwelling longwave radiative flux developed using ARM surface
531 measurements, *J. Geophys. Res.*, 113, 16, 10.1029/2008jd009936, 2008.

532 Marthews, T. R., Malhi, Y., and Iwata, H.: Calculating downward longwave radiation
533 under clear and cloudy conditions over a tropical lowland forest site: an evaluation
534 of model schemes for hourly data, *Theor. Appl. Climatol.*, 107, 461-477,
535 10.1007/s00704-011-0486-9, 2012.

536 Marty, C., and Philipona, R.: The Clear-Sky Index to separate clear-sky from cloudy-
537 sky situations in climate research, *Geophys. Res. Lett.*, 27, 2649-2652,

538 10.1029/2000gl011743, 2000.

539 Maykut, G. A., and Church P. E.: Radiation climate of Barrow, Alaska, 1962–1966, *J.*
540 *Appl. Meteorol.*, 12, 620–628, 1973.

541 Niemelä, S., Räisänen, P., and Savijärvi, H.: Comparison of surface radiative flux
542 parameterizations: Part I: Longwave radiation, *Atmos. Res.*, 58, 1–18, 2001a.

543 Orsini, A., Tomasi, C., Calzolari, F., Nardino, M., Cacciari, A., and Georgiadis, T.:
544 Cloud cover classification through simultaneous ground-based measurements of
545 solar and infrared radiation, *Atmos. Res.*, 61, 251-275, 10.1016/s0169-
546 8095(02)00003-0, 2002.

547 Prata, A. J.: A new long-wave formula for estimating downward clear-sky radiation at
548 the surface, *Q. J. Roy. Meteorol. Soc.*, 122, 1127–1151, 1996.

549 Rangwala, I., Miller, J. R., and Xu, M.: Warming in the Tibetan plateau: possible
550 influences of the changes in surface water vapor. *Geophys. Res. Lett.*, 36, 295-311,
551 2009.

552 Satterlund, D. R.: An improved equation for estimating longwave radiation from the
553 atmosphere, *Water Resource Res.*, 15, 1649–1650, 1979.

554 Stephens, G. L., Wild, M., Stackhouse, P. W., Jr., L'Ecuyer, T., Kato, S., and Henderson,
555 D. S.: The global character of the flux of downward longwave radiation, *J.*
556 *Climate.*, 25, 2329-2340, 10.1175/jcli-d-11-00262.1, 2012.

557 Stoffel, T.: Solar infrared radiation station (SIRS) handbook, Tech. Rep., ARM TR-025,
558 *Atmos. Rad. Mea. Program*, U.S. Dep. of Energy, Washington, D.C, 2005.

559 Sugita, M., and Brutsaert, W.: Cloud effect in the estimation of instantaneous downward
560 longwave radiation, *Water Resource Res.*, 29, 599-605, 10.1029/92wr02352, 1993.

561 Swinbank, W. C.: Long-wave radiation from clear skies, *Q. J. Roy. Meteo. Soc.*, 89,
562 330–348, 1963.

563 Viúdez-Mora, A., Costa-Surós, M., Calbó, J., and González, J. A.: Modeling
564 atmospheric longwave radiation at the surface during overcast skies: The role of
565 cloud base height, *J. Geophys. Res. Atmos.*, 120, 199–214, 10.1002/
566 2014JD022310, 2015.

567 Wang, K., and Liang, S.: Global atmospheric downward longwave radiation over land
568 surface under all-sky conditions from 1973 to 2008, *J. Geophys. Res.*, 114,
569 10.1029/2009jd011800, 2009.

570 Wang, K., and Dickinson, R. E.: Global atmospheric downward longwave radiation at
571 the surface from ground-based observations, satellite retrievals, and re-analyses,

572 Reviews of Geophysics, 51, 150-185, 10.1002/rog.20009, 2013.

573 Yang, K., Ding, B., Qin, J., Tang, W., Lu, N., and Lin, C.: Can aerosol loading explain
574 the solar dimming over the Tibetan Plateau? *Geophys. Res. Lett.*, 39,
575 10.1029/2012gl053733, 2012.

576 Zhao X., Peng B., Qin N., Wang W. (2011), Characteristics of Energy Transfer and
577 Micrometeorology in Surface Layer in Different Areas of Tibetan Plateau in
578 Summer (in Chinese), *Plateau and mountain Meteorology Research*,31(1), 6-11,
579 2011.

580 Zhu, M. L., Yao, T. D., Yang, W., Xu, B. Q., and Wang, X. J.: Evaluation of
581 parameterizations of incoming longwave radiation in the high-mountain region of
582 the Tibetan Plateau, *J. Appl. Meteorol. Climatol.*, 56, 833-848, 10.1175/jamc-d-
583 16-0189.1, 2017.

584

585

586 Table 1: Description of stations and measurements (magnitude and variability) at

587 three stations in the Tibetan Plateau

Site	Altitude (m ASL)	Period	T (°C)	e (hPa)	DLR ($\text{W}\cdot\text{m}^{-2}$)	Data Points
NQ	4507	2011.7.20- 2011.8.26	9.4 ± 8	7.4 ± 5	242.75 ± 40	52980
NC	2290	2014.6.7- 2014.7.31	16.8 ± 10	13.4 ± 4	368.25 ± 40	69609
AL	4279	2016.5.27- 2016.9.22	7.8 ± 4	4.8 ± 4	253.11 ± 50	86596

588

589

Table 2. 11 clear-sky DLR parameterizations and their specific conditions

Reference	Clear-Sky Parameterization	Conditions
Angstrom (1915)	$DLR_{clr} = \{0.83 - 0.18 \times 10^{-0.067e}\} \sigma T^4$	Alt.: 1650~3500 T: 283.15~303.15 e: 4~1
Brunt (1932)	$DLR_{clr} = (0.52 + 0.065\sqrt{e}) \sigma T^4$	Alt.: 6~3500 T: 269.15~303.15 e: 2.5~16
Swinbank (1963)	$DLR_{clr} = 5.31 \times 10^{-13} T^6$	Alt.: 2 T: 281.15~302.15 e: 8~30
Idso and Jackson (1969)	$DLR_{clr} = (1 - 0.261 \cdot \exp(-0.000777 \times (273 - T)^2)) \sigma T^4$	Alt.: 3, 331 T: 228.15~318.15
Brutsaert (1975)	$DLR_{clr} = 1.24 \left(\frac{e}{T}\right)^{\frac{1}{7}} \sigma T^4$	Alt.: 6~3500 T: 269.15~313.15 e: 2.5~16
Satterlund (1979)	$DLR_{clr} = 1.08 \left(1 - \exp\left(-e^{\frac{T}{2016}}\right)\right) \sigma T^4$	Alt.: 594 T: 236.15~309.15 e: 0~18hPa
Idso (1981)	$DLR_{clr} = \left(0.7 + 5.95 \times 10^{-5} \times e \times \exp\left(\frac{1500}{T}\right)\right) \sigma T^4$	Alt.: 331 T: 258.15~278.15 e: 2~6
Konzelmann (1994)	$DLR_{clr} = \left(0.23 + 0.443 \left(\frac{e}{T}\right)^{\frac{1}{8}}\right) \sigma T^4$	Alt.: 340~3230 T: 257.15~279.15 e: 1.5~5.5
Prata (1996)	$DLR_{clr} = (1 - (1 + 46.5 \frac{e}{T}) \times \exp(-(1.2 + 3 \times 46.5 \frac{e}{T})^{0.5})) \sigma T^4$	Not specified
Dilley and O'Brien (1998)	$DLR_{clr} = 59.38 + 113.7 \left(\frac{T}{273.16}\right)^6 + 96.96 \sqrt{46.5 \frac{e}{T} / 2.5}$	Not specified
Iziomon (2001)	$DLR_{clr} = \left(1 - 0.43 \exp\left(-\frac{11.5e}{T}\right)\right) \sigma T^4$	Alt.: 1489 $\bar{T} = 277.55 \bar{e} = 7.4$

591 *Where Alt. is the altitude above sea level, and its unit is (m ASL), e is screen-level water vapor

592 pressure in hPa and T represents surface temperature in K

593

594

595

596

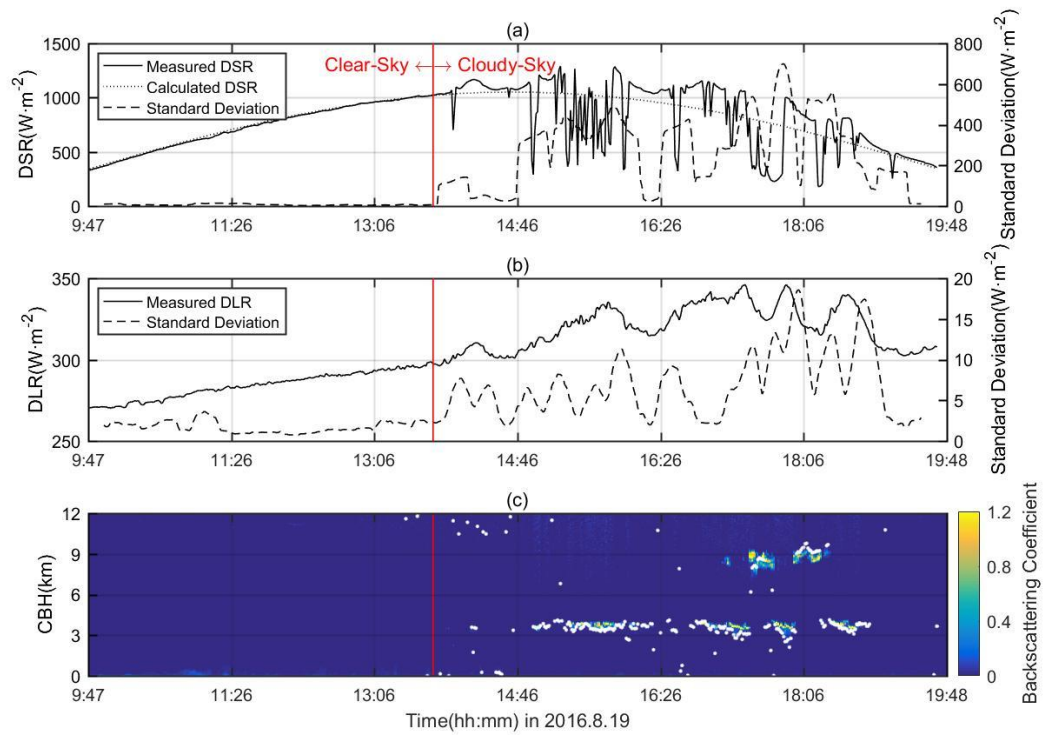
Table 3. Locally fitted clear-sky DLR parameterizations in TP

Reference	Locally fitted Clear-Sky Parameterization
Angstrom(1915)	$DLR_{clr} = \{0.8 - 0.19 \times 10^{-0.068e}\} \sigma T^4$
Brunt(1932)	$DLR_{clr} = (0.56 + 0.07\sqrt{e}) \sigma T^4$
Swinbank(1963)	$DLR_{clr} = 4.7 \times 10^{-13} T^6$
Idso & Jackson(1969)	$DLR_{clr} = (1 - 0.36 \cdot \exp(-0.00065 \times (273 - T)^2)) \sigma T^4$
Brutsaert(1975)	$DLR_{clr} = 1.03 \left(\frac{e}{T}\right)^{0.09} \sigma T^4$
Satterlun (1979)	$DLR_{clr} = \left(1 - \exp\left(-e^{\frac{T}{2016}}\right)\right) \sigma T^4$
Idso(1981)	$DLR_{clr} = \left(0.63 + 7.5 \times 10^{-5} \times e \times \exp\left(\frac{1500}{T}\right)\right) \sigma T^4$
Konzelmann(1994)	$DLR_{clr} = \left(0.23 + 0.45 \left(\frac{e}{T}\right)^{0.13}\right) \sigma T^4$
Prata(1996)	$DLR_{clr} = (1 - (1 + 46.5 \frac{e}{T}) \times \exp(-(1 + 3 \times 46.5 \frac{e}{T})^{0.5})) \sigma T^4$
Dilley and O'Brien(1998)	$DLR_{clr} = -2.54 + 158.1 \left(\frac{T}{273.16}\right)^6 + 106.4 \sqrt{46.5 \frac{e}{T} / 2.5}$
Iziomon(2001)	$DLR_{clr} = \left(1 - 0.38 \exp\left(-\frac{14.52e}{T}\right)\right) \sigma T^4$

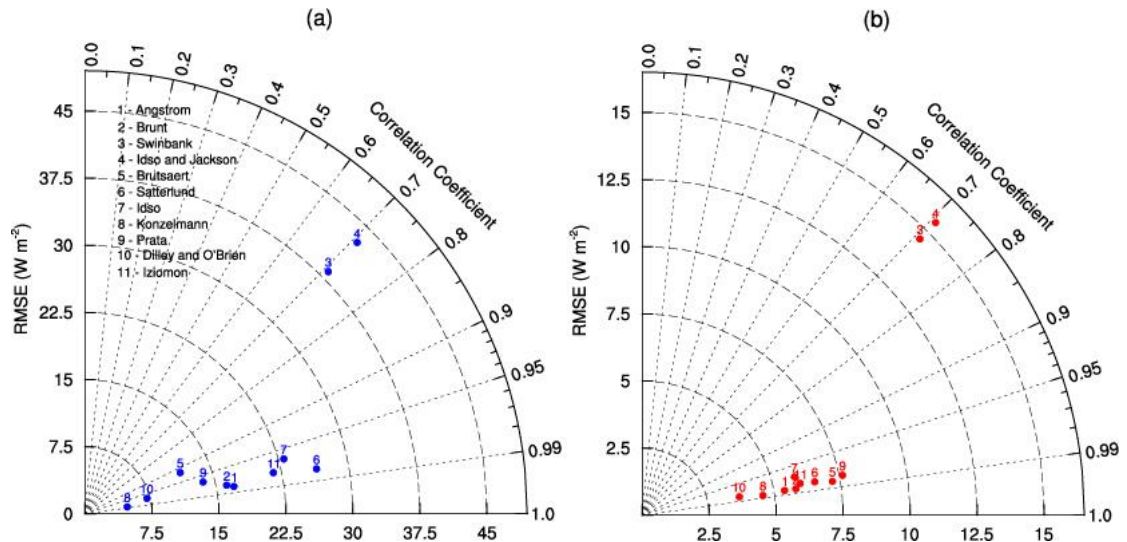
597

Table 4. 4 Ordinary and locally fitted cloudy-sky DLR parameterizations

Reference	DLR _{cl} Parameterization	Ordinary Parameters	Locally Fitted Parameters
Maykut(1973)	$(a + b \times CF^c)\sigma T^4$	a=0.7855 b=0.000312 c=2.75	a=0.85 b=0.01 c=3
Jacobs(1978)	$(1 + a \times CF)DLR_{clr}$	a=0.26	a=0.23
Sugita(1993)	$(1 + a \times CF^b)DLR_{clr}$	a=0.0496 b=2.45	a=0.2 b=1.3
Konzelmann(1994)	$(1 - CF^a)DLR_{clr} + b \times CF^a\sigma T^4$	a=4 b=0.95	a=3.5 b=1



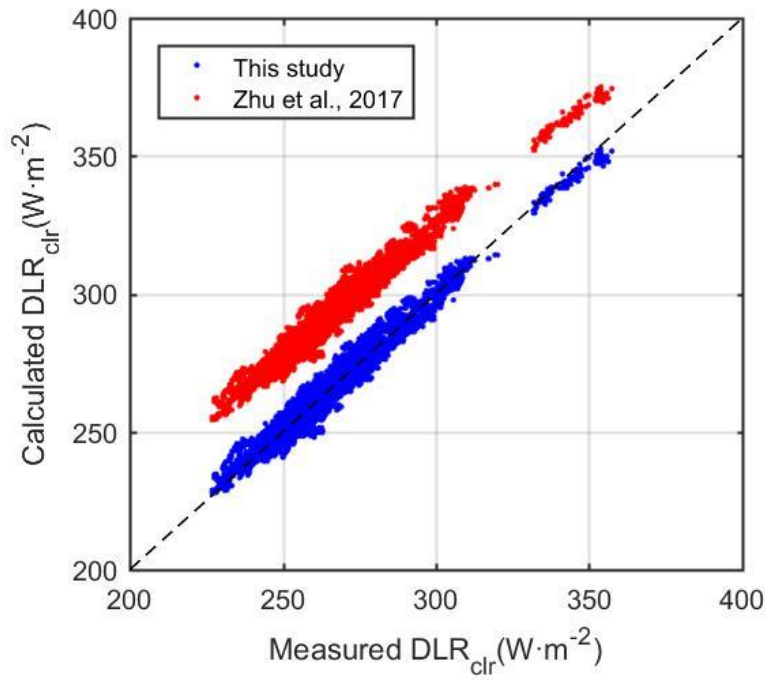
601
 602 Fig. 1. Time series of data sample on 2016.8.19 transited from clear-sky to cloudy-sky: (a)
 603 measured (black line) and calculated (dotted black line) downward shortwave radiation and its 21-
 604 min standard deviation (grey line), (b) measured downward longwave radiation and 21-min standard
 605 deviation and (c) MPL backscattering coefficient and the cloud base height.



606
 607
 608
 609

Fig. 2. RMSE and R^2 for the clear-sky DLR parameterizations using original (a) and locally calibrated (b) coefficients.

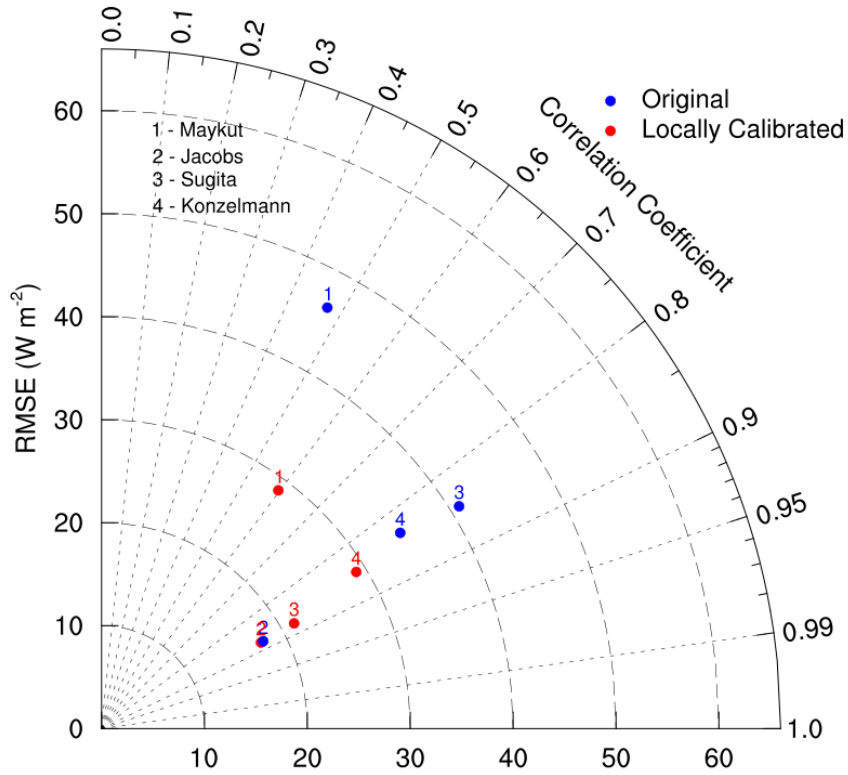
610



611

612 Fig. 3. Scatter plots of measured clear-sky DLR data from as a function of calculations
613 by the Eq.(3) this study (blue dots) and the Eq.(4) by Zhu et al. (2017) (red dots). The
614 dash black line is the 1:1 line.

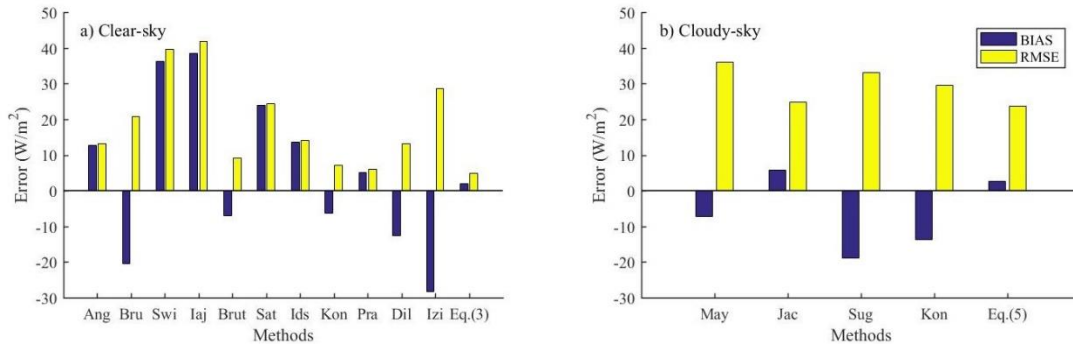
615



616

617 Fig. 4. RMSE and R^2 for the cloudy-sky DLR (DLR_{cl}) parameterizations using the
 618 original (blue) and locally calibrated (red) coefficient.

619

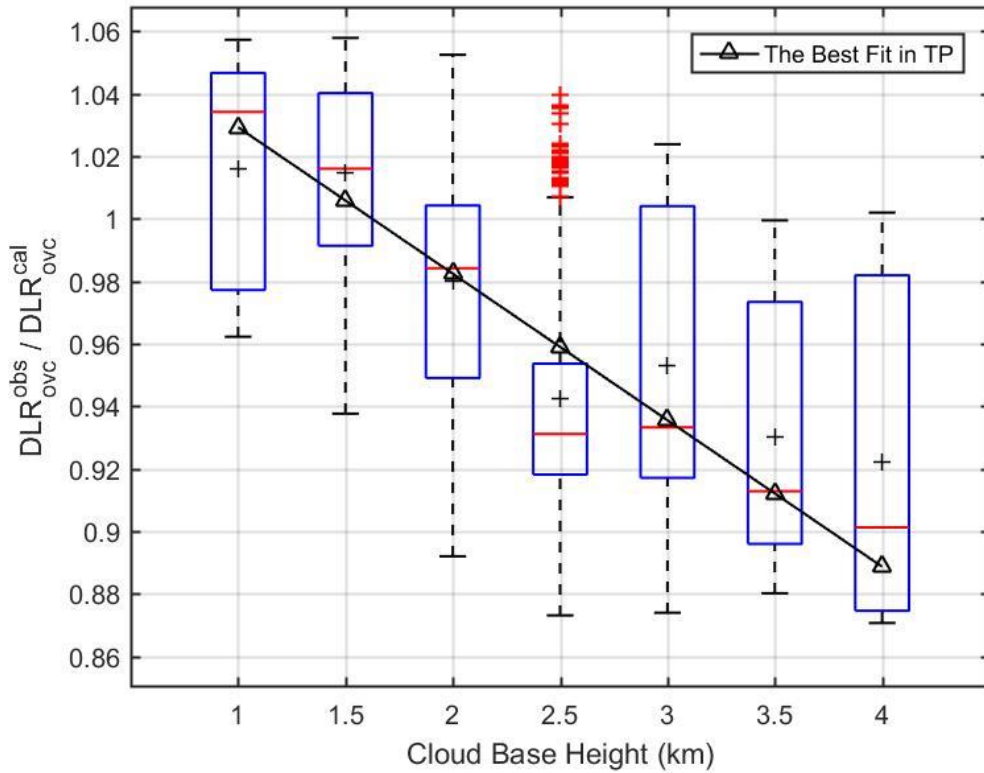


620

621 Fig. 5. BIAS and RMSE for the LDR parameterizations using (a) the published clear-
 622 sky parameterizations and Eq.(3), and (b) cloudy-sky parameterizations and Eq.(5).

623

624



626

627 Fig. 6. Distributions of the ratio of observed DLR and calculated DLR by Eq.(5) under
 628 overcast condition against measured cloud base height are represented by box plot (the
 629 blue box indicates the 25th and 75th percentiles, the whiskers indicate 5th and 95th
 630 percentiles, the red middle line is the median, the black plus sign is the mean). The
 631 black triangle line is the fitting line.